Tracking the evolution of electronic and structural properties of VO_2 during the ultrafast photoinduced insulator-metal transition

S. Wall,[1,2,*] L. Foglia,[1] D. Wegkamp,[1] K. Appavoo,[3] J. Nag,[3] R. F. Haglund, Jr.,[3] J. Stähler,[1] and M. Wolf[1]

[1]*Fritz-Haber-Institut der Max-Planck-Gesellschaft, Department of Physical Chemistry, Faradayweg 4-6, 14195 Berlin, Germany*

[2]*ICFO-Institut de Ciencies Fotoniques, Av. Carl Friedrich Gauss, 3, 08860 Castelldefels, Barcelona, Spain*

[3]*Department of Physics and Astronomy, Vanderbilt University, Nashville, Tennessee 37235-1807, USA*

(Received 29 May 2012; revised manuscript received 10 January 2013; published 20 March 2013)

We present a detailed study of the photoinduced insulator-metal transition in VO_2 with broadband time-resolved reflection spectroscopy. This allows us to separate the response of the lattice vibrations from the electronic dynamics and observe their individual evolution. When we excite VO_2 above the photoinduced phase transition threshold, we find that the restoring forces that describe the ground-state monoclinic structure are lost during the excitation process, suggesting that an ultrafast change in the lattice potential drives the structural transition. However, by performing a series of pump-probe measurements during the nonequilibrium transition, we observe that the electronic properties of the material evolve on a different, slower time scale. This separation of time scales suggests that the early state of VO_2, immediately after photoexcitation, is a nonequilibrium state that is not well defined by either the insulating or the metallic phase.

DOI: 10.1103/PhysRevB.87.115126 PACS number(s): 63.20.−e, 78.47.jg

I. INTRODUCTION

The study of the insulator-metal (IM) phase transition in VO_2 has remained an active area of research for the last 60 years.[1] At $T_c \approx 340$ K, VO_2 undergoes a first-order structural phase transition from a low-temperature monoclinic M_1 phase to a high-temperature rutile R phase. This change in the crystal structure also coincides with a five orders of magnitude decrease in resistance in single crystals, switching the material from an insulator to a metal.

The nature of the phase transition has been subject to considerable debate since its discovery. On passing from the R phase to the M_1 phase, neighboring V ions form rotated dimers along the c axis of the R phase, which doubles the number of V ions per unit cell, whilst only slightly affecting the surrounding oxygen octahedra. A schematic of the structural transformation is shown in Fig. 1. In the R phase, the crystal field splits the Vd orbitals into a lower energy t_{2g} triplet and a higher energy e_g doublet. The degeneracy of the orbitals is further split due to hybridization of the V-d levels with the O-2s and O-2p orbitals to form a broad, strongly hybridized d_{π^*} band and a less hybridized narrow $d_{\|}$ band along the c axis. These bands overlap and the Fermi energy resides within these partially filled bands resulting in metallic behavior. In the M_1 phase, the dimerization displaces the V ions away from the centers of the oxygen octahedra. This raises the bottom of the d_{π^*} band above the Fermi energy, whilst also splitting the $d_{\|}$ band.

Goodenough suggested that the structural distortion, which splits the $d_{\|}$ band, is sufficiently large to open a gap and produce the insulating state.[2] However, Mott argued that the structural distortion alone was not sufficient. Instead, the shifted d_{π^*} band resulting from the structural distortion reduces the screening of the Coulomb interaction between the electrons in the $d_{\|}$ band.[3] The narrow bandwidth of $d_{\|}$ makes it susceptible to a Mott transition and electronic correlations drive the transition to the insulating state. This view had been reinforced by the failure of density functional theory (DFT), within the LDA approximation, to reproduce the insulating nature of the M_1 crystal structure without including a Hubbard-U term. However, very recent calculations have shown that, when nonlocal exchange interactions are accounted for, the insulating and metallic phases can be obtained within DFT and additional correlation effects are not required.[4,5]

The discovery of a *photoinduced* IM transition in VO_2 has opened new avenues for investigating the transition process.[6] In these time-resolved experiments, a strong pump pulse excites the system and a second pulse probes a specific property as a function of time delay. To date, the time-dependent change in the optical reflectivity and conductivity,[7–9] as well as the electronic[10,11] and lattice[12–15] changes during the dynamic IM transition, have been measured. To drive the insulator-metal transition, an incident threshold fluence F_{TH} of approximately 7 mJ cm^{-2} has been reported when the sample is excited with 800-nm laser light at room temperature. In the linear absorption regime, this fluence corresponds to exciting approximately 1 in 10 vanadium ions, and the total deposited energy is similar to the thermal energy required to drive the phase transition in equilibrium conditions. It has also been shown that, for excitation above the optical band gap, the threshold is independent of the pump wavelength[16] and only depends on the absorbed energy density and, as expected, the threshold value is reduced when the initial temperature of the sample is increased.[7,9]

In addition, it has been observed that there are three distinct regimes for the photoinduced transition. Below F_{TH} no phase transition occurs and the material remains insulating. Above threshold, only a small region of the sample is initially transformed to the metallic phase and the dynamics are slow, being governed by the thermal diffusion of heat into the sample, which results in the growth of the metallic phase.[10] However, as the fluence is increased, the transition occurs increasingly rapidly until it reaches a saturation regime, indicating that nonthermal processes can also drive the structural transition.[12]

Cavalleri and co-workers[17] suggested that the temporal dynamics of the nonthermal photoinduced transition in VO_2 can be used to distinguish between a phase transition that is determined by Mott physics and one that is determined by the

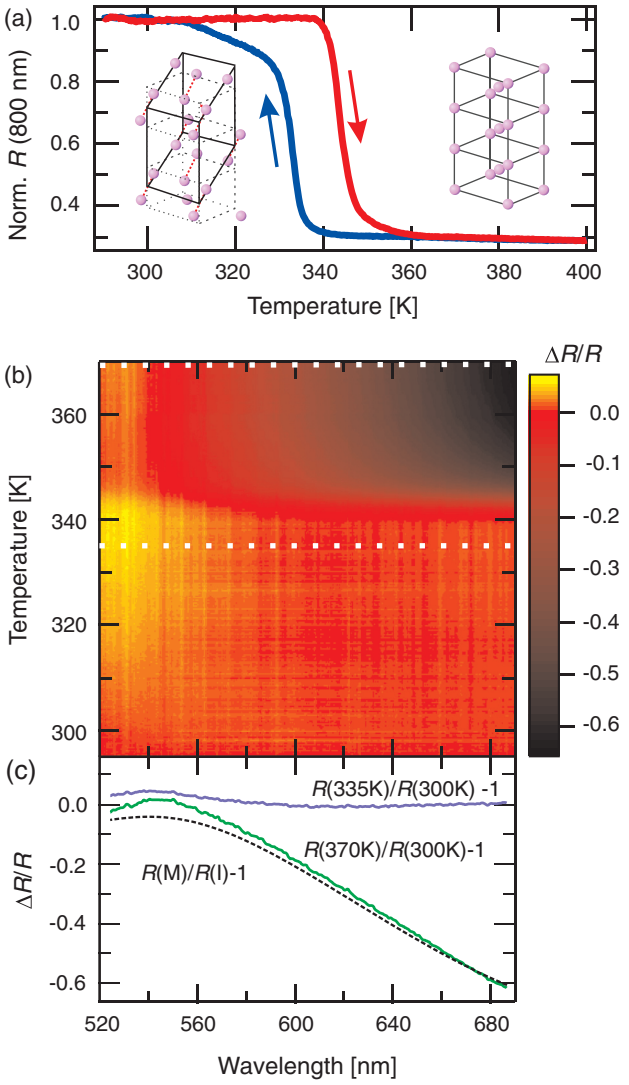

FIG. 1. (Color online) (a) Reflectivity hysteresis measured at 800 nm and corresponding crystal structures. (b) Wavelength-dependent change in reflectivity on heating, relative to the reflectivity at 300 K. (c) Cuts in the differential reflectivity spectra, corresponding to the dashed lines in (b), above and below T_c (solid lines) and expected reflectivity change based on the optical data of Ref. 21 (dashed line).

Peierls mechanism. It was argued that, if electronic correlations are responsible, then the laser excitation induces a prompt change in the screening through charge redistribution and thus the phase transition should occur promptly. However, if structural distortions alone are responsible for the insulating phase, the time scale would be set by atomic motion resulting in a slower transition. By measuring the rise time of the reflectivity transient associated with the phase transition as a function of pulse duration, the dynamics did not occur faster than a limiting 75-fs time scale. This was attributed to the time required for an optical phonon of the monoclinic phase to complete a 1/2 cycle of an oscillation, suggesting that structural motion limits the transition rate and that VO_2 was a Peierls insulator.

On the other hand, recent time-resolved diffraction experiments on the ultrafast solid-liquid transition of bismuth, which is known to be a Peierls-distorted metal, showed that the long-range order could melt on a time scale that is much shorter than that set by the phonon modes when excited with a sufficient fluence.[18] This suggests that even if VO_2 is a Peierls-distorted insulator, the time scale for the phase transition may not be limited by the phonon modes of the monoclinic phase. Testing whether such a situation occurs in VO_2 with time-resolved diffraction is more challenging as the phonon oscillations occur on time scales that are significantly faster than what can be resolved with current diffraction sources. Using time-resolved electron diffraction, Baum *et al.*[13] were able to show that the structural phase transition in VO_2 occurs over multiple time scales; first, the V ions expand, reducing the dimerization on a sub-400-fs time scale, and then untwist to the rutile-phase positions on a slower, picosecond, time scale. However, they were unable to access the 75-fs time scale of the initial step in the transition process.

To overcome this limitation, we have recently demonstrated that the change in the coherent phonon spectrum can be used as an ultrafast optical probe of the lattice symmetry.[19] Diffraction techniques measure the average positions of ions, and thus the crystal structure, by monitoring the position and number of Bragg reflections. These Bragg peaks are related to the lattice potential as it determines the equilibrium positions of the ions. The lattice potential is also related to how the atoms respond to external perturbations as it determines the restoring forces experienced by the ions when they are perturbed. These restoring forces generate the normal modes, or phonons, of the system and, when the symmetry of the structure changes, the number and frequencies of these modes also change. Therefore, by measuring the changes in the phonon spectrum in the time domain, many changes to the structural symmetry can be deduced *optically*. In addition, as measurements of the phonon spectrum are related to the forces that are experienced by the ions of the solid, these measurements may provide complementary information to time-resolved diffraction measurements regarding the nature of the structural transition.

Optical experiments can only probe the low momentum excitations in solids and are thus restricted to excitations near the Γ point of the Brillouin zone. In the monoclinic M_1 phase of VO_2 there are 18 Raman active phonon modes at the Γ point, all of which consist of motion of both the vanadium and oxygen ions, whereas the phonon spectrum of the rutile R phase consists of only four Raman active modes, which only involve motions of the oxygen ions. Furthermore, the R-phase modes are generally not observed in Raman scattering.[20] Therefore, by measuring the change in the coherent phonon spectrum, the structural changes associated with the IM transition in VO_2 can be probed optically and in the time domain.

Previously, we have used this to show that, at the high excitation densities, the phonon modes of the M_1 phase are no longer present in the excited state, suggesting that the change in the lattice symmetry is not limited by the phonon-period time scale of the M_1 phase but occurs during the excitation pulse. Thus, like bismuth, the ordered monoclinic phase of VO_2 can be also lost on a sub-phonon-period time scale. However, unlike bismuth, which melts, the final state of VO_2 is still a solid with long-range order.

The loss of the monoclinic-phase phonon modes, however, does not necessarily imply that the material has adopted the properties of the metallic rutile phase. Indeed, establishing the

metallic structure over a macroscopic volume is a slow process that takes several hundreds of picoseconds to occur.[12,13] In this paper, we examine how this out-of-equilibrium transition occurs from a structural and optical perspective. The paper is structured as follows: we start by presenting the broadband optical properties of VO_2 as it is heated across the phase transition. These thermodynamically driven reflectivity changes are compared to our previously published data on the broadband transient reflectivity changes induced by laser excitation in order to elucidate the nature of the time-dependent signals. We then go beyond our previous publication and extract specific details on how phonon modes are modified during the photoinduced transition into the metallic state. Specifically, we examine the role these modes play in the nonequilibrium insulator-metal transition. Our analysis shows that the observed phonon modes do not show any significant softening before the phase transition, demonstrating that the modes do not drive or limit the structural transition but, instead, act as an optical signature of the phase. We then address the question of whether the state of the system, after the phonon modes have been lost, can be considered as being in the metallic R phase, by examining the nature of the transient state after photoexcitation. This is achieved by comparing the pump-probe signal of the high temperature metallic state to the pump-probe signal of the transient state. We find that the emergence of the metallic state response is delayed by several hundred femtoseconds compared to the loss of the phonon modes. These results suggest that immediately after photoexcitation VO_2 is in a highly nonequilibrium state that is not characterized by either the M_1-insulating or R-metallic equilibrium phases.

II. STATIC AND DYNAMIC OPTICAL PROPERTIES OF VO_2

200-nm thick films of polycrystalline VO_2 were grown by pulsed laser deposition on an n-doped Si substrate.[22] The IM transition was observed to occur at 343 K on heating and exhibits a 10 K hysteresis width, as deduced by the change in reflectivity at 800 nm [see Fig. 1(a)]. The broadband (520–690 nm) reflectivity change during heating is shown in Fig. 1(b). For probe wavelengths longer than 600 nm, the reflectivity is largely temperature independent before the phase transition. Only wavelengths shorter than 600 nm show a small increase in reflectivity. On crossing the critical transition temperature, a large decrease in reflectivity is observed at all wavelengths, the magnitude of which is particularly large at longer wavelengths. The change in reflectivity is consistent with the optical model reported in Ref. 21. Figure 1(c) compares the measured change in reflectivity between the insulating state, $T = 300$ K, and the metallic state, $T = 370$ K (solid green line), to the change in reflectivity for a thin film on VO_2 on a Si substrate (dashed black line) using the parameters for the dielectric function measured in Ref. 21. This model assumes that longer wavelengths probe transitions between the $d_{\|}$ bands and thus are strongly affected by changes in the number of free carriers around the Fermi level. On the other hand, shorter wavelengths probe transitions between the O-2p to V-3d_{π} states, which are less affected by the phase transition. Therefore, in the time-resolved measurements, longer wavelengths should be more sensitive to the change in the population of carriers, whereas shorter wavelengths should be more sensitive to changes in bond angles that affect dipole transition probabilities.

These temperature-induced effects on the reflectivity are particularly important for understanding the transients observed during the photoinduced insulator-to-metal phase transition. Figure 2 summarizes our previously published results[19] on photoexcited VO_2. These measurements were performed at room temperature when VO_2 is in its insulating monoclinic M_1 phase. The sample was excited with a p-polarized 800-nm, 40-fs pump pulse with an angle of incidence of approximately 50°. The reflectivity change was probed both with a broadband source as well as with a second 800-nm pulse, which made a small angle to the pump pulse. The transient reflectivity measured at 800-nm was performed at a repetition rate of 150 kHz and the probe pulse had s-polarization in order to minimize coherent interference between the two pulses on the sample, and the reflectivity change was measured with a diode and lock-in amplifier. Broadband pulses were generated by focusing part of the 800-nm fundamental beam into a YAG crystal to produce white light with p-polarization that was then compressed by a deformable mirror to less than 20 fs as described in Ref. 23. The spectrally resolved measurements of Figs. 2(a) and 2(b) were acquired using a spectrometer and the unperturbed signal at negative time delays is used to normalize the data. The narrow-bandwidth measurements at 525 nm, shown in Fig. 2(d), were obtained by spectrally filtering the probe pulse to 5 nm after reflection from the sample, in order to preserve the time resolution, and detected using a diode and a lock-in amplifier with a repetition rate of 100 kHz. This reduction in repetition rate for the white light measurements enabled more time for the system to recover and cool between pump pulses, reducing average heating effects and allowing the system to be excited with higher fluences using the same laser system. Thick (200-nm) films of VO_2 ensure that the 800-nm pump pulse, which has a penetration depth of less than 180 nm,[21] does not significantly excite the substrate.

Figure 2(a) shows the early transient dynamics of the photoexcited M_1-phase VO_2 when excited below the photoinduced IM transition threshold. Pronounced oscillations are observed across the entire probed spectrum. As previously discussed, these modes correspond to the reflectivity change induced by the coherent oscillations of the 5.7- and 6.7-THz phonon modes of the monoclinic M_1 phase.[19] In addition the background value, about which the reflectivity oscillates, also changes. Longer probe wavelengths show a large decrease in background reflectivity, which recovers on a few-hundred-femtosecond to picosecond time scales, whereas probes at shorter wavelengths show an increase in reflectivity with much slower dynamics.

Figure 2(b) shows the broadband reflectivity change when VO_2 is excited with a pump fluence above the photoinduced IM transition threshold. In this regime, the dynamics that results is appreciably different from the below threshold case. Although the decrease in reflectivity is still the largest at the longest wavelengths probed, the decrease is now observed over the entire probed wavelength range. In addition, the oscillations are no longer present and the time scales of the dynamic has changed.

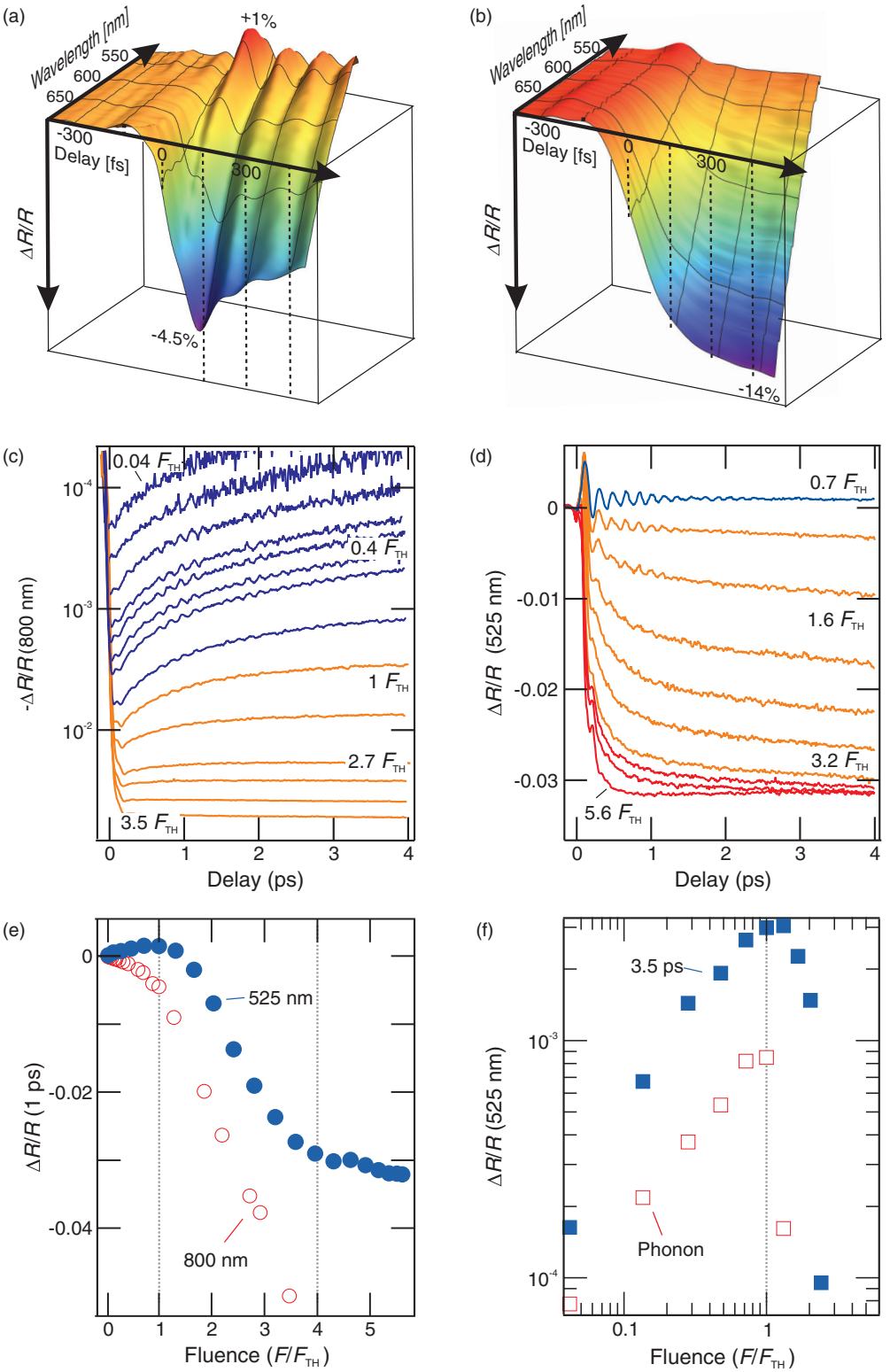

FIG. 2. (Color online) Broadband reflectivity change, measured at room temperature (a) below the photoinduced IM transition threshold pumping and (b) above.[19] Change in reflectivity at (c) 800 and (d) 525 nm measured for a range of fluences above and below threshold. Blue lines correspond to pump powers below threshold, orange above, and red in saturation. (e) Power dependence of the reflectivity change at 1 ps measured at 525 and 800 nm plotted against a normalized fluence scale. Vertical dashed lines indicate the transition threshold and saturation regimes. (f) Comparison of the reflectivity change at 3.5 ps, when the coherent phonon amplitude has reduced, to the "amplitude" of the phonon signal, as measured by the difference in reflectivity between the first trough and the following peak.

Time-resolved broadband spectroscopy is a powerful tool for determining the nature of the dynamics in complex materials[24–26] and for the study of optically induced phase transitions,[27] as the broadband change in reflectivity can be used to fit the time-dependent parametrization of the static dielectric function. This is difficult in VO_2 as there are several broad spectral features overlapping in this regime.[21] However, the qualitative assignments based on static, temperature-dependent properties are still valid, i.e., transitions probed by longer wavelengths are sensitive to changes in the number of carriers close to the Fermi level, whereas transitions at shorter wavelengths are more sensitive to structural effects relating to modulation of the O-2p–V-3d_π hybridization.

Therefore, for the rest of this study we focus on the two extrema of Figs. 2(a) and 2(b) in order to make a more quantitative analysis of the photoinduced transition. Figures 2(c) and 2(d) show the transient reflectivity at 800 and 525 nm, respectively, over a wide range of pump fluences. Here, the contrast between the dynamics observed at the two wavelengths is clear, demonstrating that different phenomena are probed by the different wavelengths: namely, the dynamics at 800 nm is more sensitive to the changes in the number of carriers, whereas the dynamics at 525 nm is more sensitive to the structure.

Below threshold, the reflectivity change at 800 nm is clearly dominated by a double exponential recovery, on top of which there are small oscillations. These exponential transients are not observed in the data at 525 nm, which instead show a positive steplike response and large-amplitude oscillations.

Above threshold, the magnitude of the change in reflectivity dramatically increases with increasing pump fluence and, at longer time delays, a second peak in the transient reflectivity was observed at both wavelengths after about 100 ps, which is not shown here. On increasing the pump fluence further above threshold, the secondary peak was observed to arrive sooner. The long-time-scale dynamic is associated with a thermal transition to the metallic R phase, as the pump pulse delivers enough energy to drive nucleation locally within the probed region, leading to a volume expansion, which has been observed with time-resolved x-ray diffraction.[12]

As the pump intensity is increased, the magnitude of the reflectivity change continues to increase until approximately $4 \times F_{\mathrm{TH}}$, at which point the signal starts to saturate, indicating a nonthermal change of the entire probed volume. These three regimes, below threshold, above threshold, and saturation, can be clearly seen in the fluence dependence of the reflectivity shown in Fig. 2(e), where they are marked by dashed lines.

In order to remove systematic errors in the measurement of the absolute fluence of each data set, we assume that the threshold for the photoinduced transition is independent of the probe wavelength and define it as the point at which nonlinear effects appear in the transient reflectivity signals at 1 ps. Figure 2(e) shows the reflectivity at a pump probe delay of 1 ps for both wavelengths plotted on a normalized fluence scale. This normalization removes an accumulation of small errors such as an inaccurate determination of the pump spot size, different absorption and reflection losses due to different angles of incidence, and absorption properties[28] or small inhomogeneities within the sample, which arise when comparing the two data sets taken at different times. By taking the mean and standard deviation of the threshold values of each data set, we obtain a photoinduced threshold of 5.5 ± 0.6 mJ cm^{-2}, in good agreement with previous measurements.[29]

In our previous publication,[19] we proposed that the phonon modes act as a marker for the M_1 phase and that their disappearance is an indicator for the photoinduced transition to the metallic state. This is shown in Fig. 2(f), where the phonon mode amplitude, defined as the difference in the reflectivity change between the first trough and the following peak, is plotted as a function of the pump fluence. Initially, the phonon amplitude shows a linear power dependence with the pump fluence; however, on crossing the threshold fluence, the phonon signal reduces and then becomes negative, indicating the loss of the phonon mode. At the same time, the slower background reflectivity change at 3.5 ps also shows the same trend.

In the following section, we examine how these phonon modes evolve as the photoinduced phase transition is approached with increasing excitation fluence. In particular, we examine whether a softening of the phonon modes at the Γ point plays a role in the nonequilibrium transition.

III. LOSS OF THE MONOCLINIC PHASE

As discussed previously, the M_1 phase has 18 Raman active phonon modes of which nine have A_g symmetry that can be easily excited as coherent phonons. Out of these, two modes at 5.67 and 6.7 THz are particularly strong in Raman scattering and are the strongest modes that we observe. These modes act as an indicator for the M_1 phase as they involve motions of the oxygen and vanadium ions, whereas the metallic rutile phase has four Raman active phonon modes, of which only one is A_g symmetric and only involves motions of the oxygen octahedra. However, these Raman active modes are generally overdamped and not observed in Raman scattering measurements. In this section, we seek to examine quantitatively how these modes change as function of the excitation fluence in order to elucidate the role of the structural dynamics during the transition.

A. Modeling the dynamics

Photoexcitation at 800 nm excites electrons across the optical band gap generating carriers and modifying the charge distribution. The resulting carrier dynamics, such as carrier recombination and carrier diffusion, changes the occupancy of states in the solid, which in turn modifies the optical reflectivity. In addition, the change in the charge distribution modifies bond strengths, leading to a change in the forces experienced by the ions and causes them to move from their equilibrium positions. This affects the wave-function overlap and thus the dipole transition probabilities between the states sampled by the probe pulse and thus also modifies the reflectivity. These effects result in nonthermal changes in the reflectivity, however, as the system thermalizes, the change in reflectivity should begin to resemble the effects induced by heating.

In lieu of a theoretical description for the dielectric response of VO_2, we adopt a semiempirical model to quantify the dynamics in which we partially separate the carrier generation, lattice and heating contributions to the change in reflectivity.

We start by examining the lattice contribution to the reflectivity change. Following the scheme described in Ref. 30 for the displacive excitation of coherent phonons, the force exerted on the ions F_e is directly proportional to the number of excited electrons generated by the laser pulse, n_e, which obey the following rate equation:

$$\dot{n_e} = P(t) - \frac{n_e}{\tau_e}, \tag{1}$$

where $P(t)$ is the rate of electron transfer, set by the intensity profile of the 800-nm pump pulse, and τ_e is the decay rate of the electrons that generate the force on the lattice.[31] When the excitation fluence is below threshold and the induced force on the lattice is small, the response of the lattice can be described in terms of the normal modes, or phonon coordinates, which satisfy the following equations of motion:

$$\ddot{q_i} + 2\zeta_i\omega_i\dot{q_i} + \omega_i^2 q_i = \alpha_i F_e(t), \tag{2}$$

where q_i is the displacement of the Q_i mode from the equilibrium position, $\omega_i = 2\pi f_i$ is the phonon frequency, ζ_i is the damping ratio, and α_i is a coupling constant between the normal mode and the force and is nonzero only for the A_g-symmetric Raman-active phonons. The phonon displacement then affects the reflectivity R by

$$\Delta R_Q(\lambda,t) = \sum_i \frac{\partial R(\lambda)}{\partial Q_i} q_i(t). \tag{3}$$

Therefore the time dependence of the phonon displacement is independent of the wavelength at which it is probed.

If the time over which the force is applied is fast compared to the phonon frequencies, the lattice is driven nonadiabatically as it cannot keep up with the change in the equilibrium position. This causes the structure to "ring," i.e., coherent phonons are generated. In the displacive mechanism for coherent phonon generation, the force is persistent, τ_e is large, and the ions oscillate around new, displaced, positions and the phonon modes have a cosine-like phase, whereas in the limit $\tau_e \to 0$, the force is impulsive resulting in zero net change in the equilibrium position but sine-like oscillations are generated about the equilibrium position. Therefore, in the displacive regime, there are two, connected, contributions to the phonon-induced reflectivity change. The first is associated with the displacement of the equilibrium position, the second with the coherent oscillations. The impulsive limit, on the contrary, only consists of the oscillatory response.

Firstly, we address the nature of the force on the phonon modes. To do this, we numerically integrate Eq. (2) and do not separate the oscillations from the shift in the equilibrium coordinate as is usually the case when analyzing the coherent phonon signal. This allows us to determine some temporal properties of the forces exerted on the ions. As we do not observe any exponential decay in the data at 525 nm, we can rule out an intermediate decay constant ($100 \lesssim \tau_e \lesssim 4$ ps) for recovery of the phonon equilibrium position, thus neither of the exponential decay terms observed in the 800-nm data can be assigned to the recovery of the equilibrium position of the lattice. In addition, as the change in the equilibrium phonon position is connected to the phonon oscillation amplitude, we can also rule out a steplike force ($\tau_e \to \infty$) as we would expect a much larger offset in both the 525- and 800-nm data. From fitting both data sets using the model described below, with τ_e as an adjustable parameter, we found that $\tau_e = 50$ fs gave the best fit for all fluences and was thus held fixed for a subsequent iteration of the fits.

In addition to the lattice dynamics, there are also carrier dynamics observed in the 800-nm data as well as heating effects. These terms give a change of reflectivity, which we describe as

$$\Delta R_E(\lambda,t) = \Theta(t)\left[\sum_j B_j(\lambda)e^{-t/\tau_{B_j}} + H(\lambda)\right], \tag{4}$$

where B_i is the amplitude and τ_{Bi} the decay rate of the electronic terms. H is a time-independent heating term. Although this term is not truly time dependent, it represents the semiconstant value the reflectivity reaches after several picoseconds and decays on much longer time scales. All fitted terms depend on the probe wavelength. $\Theta(t)$ is a sigmoid function that will be discussed in more detail later.

The total change in the reflectivity is then given as the sum of Eqs. (3) and (4). After a first round of fitting, where all parameters were allowed to vary, it was found that the time constants τ_{B_i} were independent of fluence and were held constant at $\tau_{B_1} = 250$ fs and $\tau_{B_2} = 1.42$ ps for a subsequent iteration of the fit.

An example of the fitting result, in the low-fluence regime, is shown in Fig. 3(a) for both the 800- and 525-nm data sets. We find that, in this regime, an excellent fit to the data is achieved with two phonon modes, a constant heating term and, in the 800-nm data only, two exponential decays, i.e., $B_i(\lambda = 525\text{ nm}) = 0$. The quality of the fit across the whole measurement window is demonstrated by the flat residual shown for both fits. The Fourier transform of the residual signal is shown in the insert of Fig. 3(a) and shows that, in addition to the two fitted modes, we also observe a low-amplitude oscillation at 10 THz in the data at both wavelengths and an additional peak at 4.3 THz was also observed in most of the 800 nm data sets, but was less reproducible. These additional modes are also A_g Raman active modes that are also observed in Raman scattering.[20,32] In principle, these modes can also be used to track the phase transition, however, as their perturbation on the reflectivity is significantly lower than the two modes at 5.6 and 6.7 THz, they will not be discussed further.

Below threshold, the amplitudes of B_i terms in the 800-nm data were found to be linearly dependent on fluence and are not reproduced here. Instead we focus on the fluence dependence of the 5.7- and 6.7-THz phonon parameters. Figures 3(b)–3(d) show the amplitude A, damping ratio ζ, and frequency f of the two modes fitted in the below threshold regime measured at 800 (open markers) and 525 (filled markers) nm. The phonon amplitude A combines all the parameters related to the amplitude of the phonon displacement in Eqs. (2) and (3). The fluence dependence of the phonon amplitude [see Fig. 3(b)] shows the same trend as that extracted from the raw data [see Fig. 2(f)], suggesting the fit accurately captures the dynamics. The parameters ζ and f should be intrinsic to the lattice vibrations and thus independent of the probe wavelength. This trend is roughly reproduced by the fitting, where both parameters follow the same trend as a function of pump fluence. However, the 800-nm data systematically

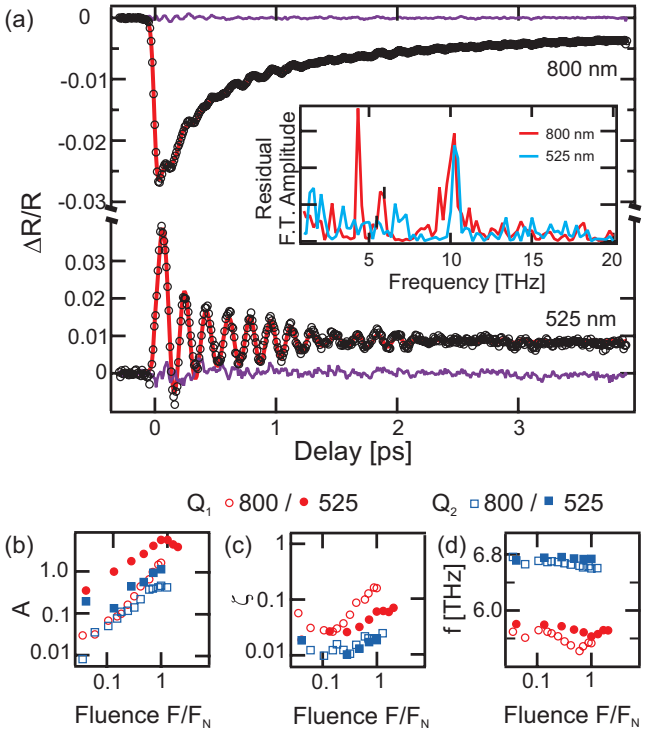

FIG. 3. (Color online) (a) Examples of fits in the below threshold regime for 800-nm (upper) and 525-nm (lower) transient reflectivities (circles: data, red lines: fits, purple lines: residuals). The insert shows the Fourier transform of the residual signal exhibiting modes at 4.3 and 10 THz. (b)–(d) The fluence dependence of the phonon mode parameters: A is a phonon amplitude, ζ is a damping ratio, and f is a phonon frequency in the low-fluence regime. Filled (unfilled) markers correspond to parameters from 525(800)-nm data. Circles correspond to the parameters associated to the Q_1 mode, squares correspond to Q_2. The errors in the fit parameters are discussed in the text.

show higher damping rates and lower frequencies than the data recorded at 525 nm.

The error in the fit is difficult to determine. The values and trend for the phonon parameters were found to be the same even with slight changes to the models, such as longer or shorter force constants on the phonon modes. Within the given model, with all parameters left free, the standard deviation of the fit parameters was found to be less than the size of the marker used in the figures. However, this error does not accurately reflect the true uncertainty as, due the nonlinear nature of the fit, a change in one parameter can often be compensated for, to some degree, by a change in another. This is particularly true for the data recorded at 800 nm where there are 11 free parameters (2×3 parameters for the phonon modes, 2×2 parameters for the carrier dynamics and one term for the heating). In addition, two further phonon modes can be seen in the data and are not included in the fit but also influence the result. This problem is reduced in fits of the data recorded at 525 nm where there are only seven free parameters (2×3 parameters for the phonon modes and a heating term) and the strength of additional phonon modes is significantly weaker. As a result, the fittings in the visible region should be more the accurate parameters, and the fit results at 800 nm should be considered as providing more of a qualitative confirmation.

In this below-threshold regime, the reflectivity change induced by the lattice motion is larger when measured at 525-nm than at 800 nm for both phonon modes. This suggests that the transitions between the O-2p to V-d_{π^*} are strongly modulated by the coherent phonons. On increasing the pump fluence, the amplitudes of the modes increase linearly until the transition threshold. Over the same fluence range, and in both data sets, the frequency of the higher energy 6.7-THz mode remains approximately constant, whereas the lower frequency 5.7-THz mode softens by approximately 3%. Interestingly, the softening of 5.7-THz mode is not observed during heating,[33,34] suggesting that this mode in particular may couple more strongly to the photoexcited electrons and be more sensitive to disorder.

Importantly, we find that $\zeta \ll 1$, even when approaching the fluence required to drive the IM transition, indicating that the phonon modes remain underdamped. As the system does not show any sign that it is driven into the overdamped regime, this supports our previous conclusion that the M_1-phase zone-center phonon modes do not limit the phase transition.[19]

The description of the reflectivity dynamics above fits well for all fluences below the threshold. However, at higher fluences, the model is unable to accurately describe the data, thus making it harder to ascertain the role of overdamped phonons during the transition. The difficulty to model this transition is twofold. The above threshold regime is inhomogeneously excited due to the finite penetration depth of the pump pulse, resulting in some regions of the film at above threshold and some below. This results in a mixed response of the two regimes as well as strong thermal diffusion, which does not occur in the other two regimes. This can be clearly seen by the dramatic change in Fig. 2. It is particularly clear in the 525-nm data, where a slow negative component in the reflectivity emerges above threshold and speeds up with time. In addition, we observe the 5.7-THz mode to restiffen at the highest fluences. We believe that this is a strong indication that we are probing an inhomogeneously excited film. Photoexcitation decreases the reflectivity so dynamics from back of the film contributes more to the measured reflectivity change. When the film is excited with a total fluence close to threshold fluence, the back side will be excited with a fluence which is still below threshold, whereas the front surface, which undergoes the transition, will not generate coherent phonons, thus resulting in a measurement of a phonon with slightly higher frequency than would be expected.

The second issue is that, if the material enters an overdamped regime, i.e., $\zeta \gg 1$, ζ and ω are strongly coupled making it hard for Eq. (3) to converge if both parameters are allowed to vary freely. Therefore, in order to test if the phonon modes enter the overdamped regime when excited at fluences, which saturate the transition, we modify our model. Since the changes in the dynamics are most clear when probed at 525 nm, we focus on this wavelength region. If the phonon modes become overdamped, the solutions of Eq. (2) change from harmonic functions to decaying exponentials. For simplicity, we model this scenario phenomenologically as

$$\Delta R_s = \Theta(t)\left(\sum_{i=1,2} C_i e^{-t/\tau_{C_i}}\right). \quad (5)$$

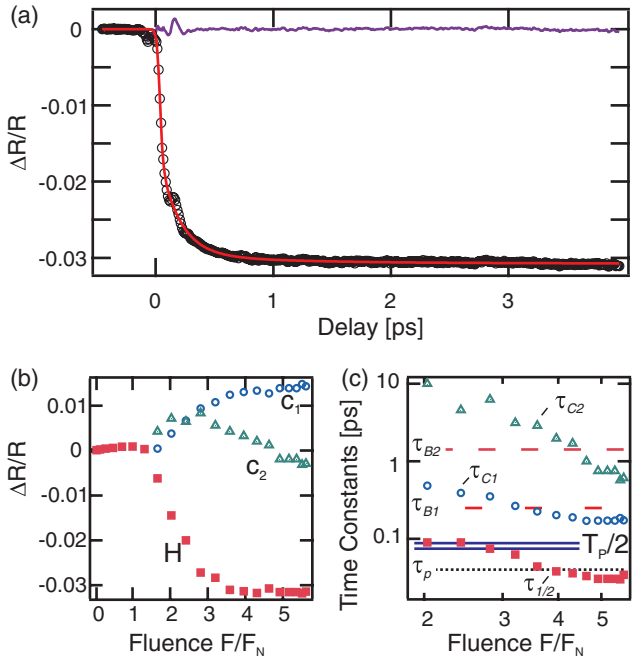

FIG. 4. (Color online) (a) Example fit in the above threshold regime for a 525-nm probe wavelength (pump fluence $4.7F_{TH}$), (circles data, red line fits, purple line residual). (b) The fluence dependence of the heating term, H (filled squares), C_1 (open circles), C_2 (open triangles) from fitting Eq. (5) on a linear scale. (c) Half-rise time $\tau_{1/2}$ (solid squares), time constants τ_{C1} (open circles), and τ_{C2} (open triangles) are displayed on a log-log scale. Dashed red lines correspond to the time scales observed in the 800-nm data below threshold. The solid lines correspond to the time for a half period, $T_p/2 = 1/2f$ of the 5.7- and 6.7-THz phonon mode and the pulse duration. Dashed black line, $\tau_p = 40$ fs, corresponds to the pulse duration.

If these decaying exponentials result from damped phonon modes, C_i would correspond to the amplitude and τ_{C_i} is related to the damping of the phonon modes. It should be noted that the more overdamped a mode is the slower it responds. The sigmoid function $\Theta(t) = \{1 + \exp[-(t - \tau_{1/2})/w]\}^{-1}$ is used to capture any delayed response associated with the phase transition such as the structural bottleneck reported in Ref. 17, where $\tau_{1/2}$ is the half-rise time of the signal and w is related to the rate.[35] To fit the reflectivity transients in the saturated regime, Eq. (5) was used together with the heating term from Eq. (4). In the intermediate regime, where the phonon modes were still observable, Eq. (3) was also included.

Figure 4 shows a typical result of the fit in the saturation regime and the fluence dependence of the fit parameters. The model provides a good fit to the data in the saturation regime, with the exception of a small spike near time zero, which we attribute to a coherent artifact, which is common in broadband measurements.[36,37] In particular, the heating term H, shown in Fig. 4(b), follows the same trend as the measured reflectivity at 1 ps shown in Fig. 2(e); it initially shows a positive growth followed by a negative response that saturates. All three time constants fitted decrease with increasing pump intensity. The amplitude of the slowest term C_2, which corresponds to dynamics on time scales of several picoseconds, grows and then decreases as the fluence increases. This term is likely to capture elements of the thermal growth of the R phase into the probed volume, which becomes less important when the excitation density is in the saturation regime. Therefore it is unlikely that this term is connected to the damping of any phonon mode.

The faster C_1 term consists of dynamics that occur over hundreds of femotseconds. This term becomes increasingly important in the saturated regime and is most likely related to the nonthermal transition. While the exact origin of this term is unknown, the fluence dependence of the time constant also allows us to rule out an overdamped response of the phonon modes as the explanation. If the phonon modes became overdamped, the response of the system would become *slower* as the increased rate of damping resists the motion of the ions. If the pump pulse increased the damping rate of the phonon, we would expect the time constants observed in Fig. 4(c) to increase with increasing pump fluence.

In addition, below the saturation threshold, $\tau_{1/2}$, which defines the onset time for the saturation regime, is similar to the half-period of the two observed phonon modes and may correspond to the bottleneck time scale observed in Ref. 17. However, on increasing fluence, this time constant approaches and crosses that of the pulse duration of the exciting laser (40 fs), suggesting that the IM transition can be driven arbitrarily fast and that the bottleneck time scale does not limit the transition at the highest excitation fluences. We emphasize that the model presented for the saturation regime is only phenomenological and is intended to demonstrate the change in the time scales observed, particularly the increasing speed at which the dynamics occurs. However, although we do not wish to assign these time scales to specific phenomena, we point out that the increasing rapid changes are incompatible with a softening of the phonon modes and no bottleneck time scale is observed in the reflectivity data at 525 nm for the highest excitation fluences.

These results together suggest that strong photoexcitation by the pump laser pulse has a dramatic and ultrafast impact on the lattice potential experienced by the phonon modes. We have presented clear evidence that the phonon modes do not exhibit a strong damping effect in the photoinduced transition, and instead the optical response suggests that the photoexcitation raises the symmetry of the lattice potential on an ultrafast time scale as observed by the vanishing of the M_1 modes. However, although the loss of the restoring forces of the M_1 phase occurs promptly, the system is still far from equilibrium and although the lattice potential has changed, the electronic properties may not. In the next section, we examine the formation of the metallic state from an optical perspective.

IV. EVOLUTION OF THE METALLIC STATE DURING THE ULTRAFAST TRANSITION

Determining when the metallic state "forms" is difficult in an out-of-equilibrium situation, as many processes occur such as volume expansion and thermal diffusion, which act in addition to the changes associated with the phase transition. In order to minimize these effects, we perform a pump-probe experiment on the *transient* state of VO_2, i.e., by performing an additional pump-probe measurement after driving the

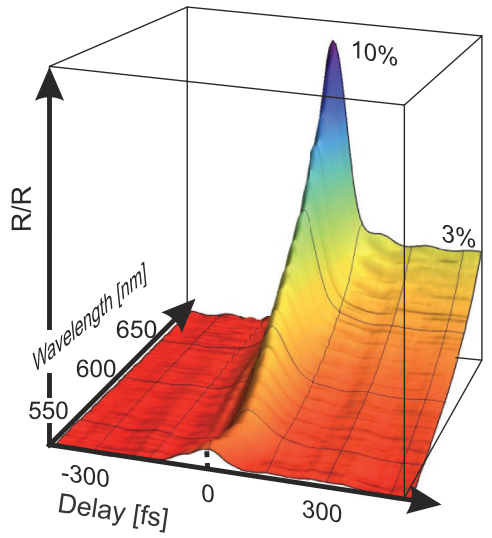

FIG. 5. (Color online) Broadband pump-probe signal of metallic VO_2 at 400 K. The response is characterized by a positive spikelike change in reflectivity at all wavelengths and a slower scale dynamics on longer time scales which is larger at longer wavelengths. Note that the wavelength axis has been swapped compared to Fig. 2.

transition with an intense first pulse. By studying the response of photoexcited VO_2, we can track the material changes as the system transforms from the insulating state into the metallic state whilst being less sensitive to other phenomena not directly related to the transition.

The response of the equilibrium metallic phase to photoexcitation is markedly different to that of the low temperature phase. Figure 5 shows the broadband response of the metallic R-phase of VO_2 at 400 K. Unlike the insulating phase, metallic VO_2 shows an increase in reflectivity at all wavelengths after photoexcitation. In particular, it is characterized by a sharp spikelike increase in reflectivity near zero time delay and then a slower transient. The transient signal was observed to scale linearly with pump fluence as there is no further phase transition to induce. To date, the metallic R phase pump-probe response of VO_2 has received little attention and we do not attempt to make a definitive assignment of the dynamics here. The R phase of VO_2, statically, is not described by the behavior of a typical metal, thus making the dynamics difficult to interpret. However, we note that the spikelike response would be consistent with either a rapid decay of hot carriers or with the response of an overdamped phonon mode of the metallic R phase. Our aim, in this section, is to use the temporal profile of the reflectivity change of the metallic phase, in response to a pump pulse, as an optical marker for the formation of the metallic state from the insulating state.

To probe the *transient* state, we generated two pump pulses by inserting a Mach-Zehnder interferometer into the pump beam path. This produces two collinear pump pulses that are separated by a variable delay. The zero time delay between the two pulses was accurately determined by measuring the interferometric autocorrelation of the two pump pulses on the VO_2 sample by a third probe pulse that measured the nonlinear induced reflectivity change at a long delay.

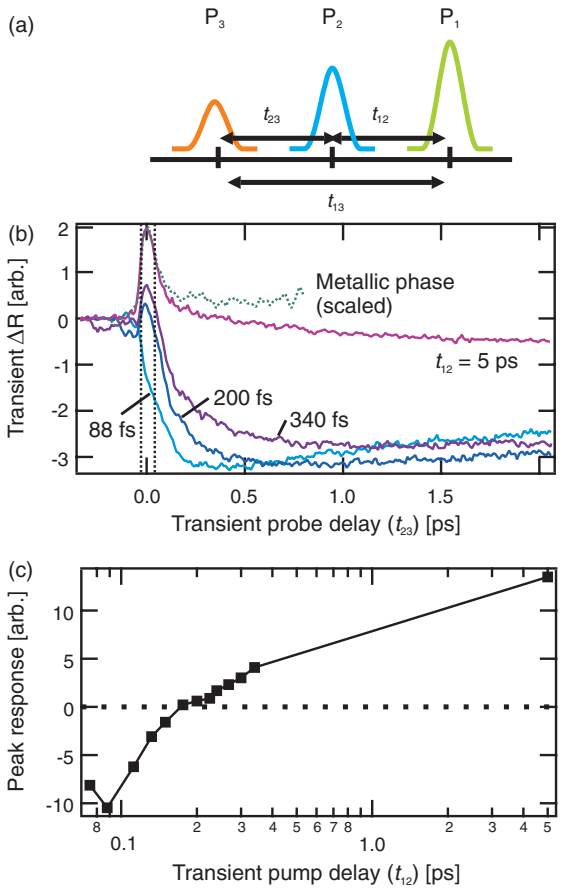

FIG. 6. (Color online) (a) Pulse sequence used to probe the formation of the metallic state. P_1 is above the threshold fluence and triggers the transition, P_2 excites the transient state after a time t_{12}, and the response is probed by P_3. (b) Pump-probe measurements on the induced reflectivity change in the transient state compared to the metallic state response at 525 nm. The numbers correspond to the delay between the P_1, which creates the transient state and P_2, which excites it. Dotted line corresponds to pump-probe signal in the metallic state. (c) Formation of a metallic peak response, data points are obtained by integrating the area between the dashed lines in (b).

In these experiments, the first pump, P_1, is above the threshold and creates a transient state S_T, which will eventually thermalize to the metallic R state. After a time delay, t_{12}, a second pulse, P_2, excites the transient state of the system to create a new excited state S_e. This combined response of both pumps is probed at a time t_{13} after the first pump pulse by a third pulse, P_3, which measures the combined change in reflectivity $\Delta R_c = \Delta R_T + \Delta R_e$ arising from the reflectivity change associated with the two excitation pulses. A schematic of the pulse sequence is shown in Fig. 6(a). To obtain the transient response of the excited state, we subtract the transient reflectivity that results from a single pump pulse (corresponding to P_2 with zero intensity) from the measured double pump transient data.

Figure 6(b) shows the temporal change in reflectivity of the excited state for different time delays after the creation of the transient state (different t_{12} delays), plotted as a function of delay between P_2 and the probe t_{23}.

The excited response varies significantly as the underlying transient state evolves. At early times, just after the creation of the transient state, the excited state shows a further decrease in reflectivity and partial recovery on a picosecond time scale. As the system further evolves, a positive spike in the transient reflectivity change is observed at early times, although the signal is still dominated by a decrease on longer time scales. It is not until several picoseconds have passed that a response that begins to resemble the metallic state [dashed line in Fig. 6(b)], i.e., a positive contribution to the reflectivity at early times and no negative response, is observed.

To quantify this evolution, we plot the integrated reflectivity change in the vicinity of $t_{23} = 0$, i.e., the time at which the positive peak of the reflectivity is at a maximum in the metallic phase in Fig. 6(c). As can be clearly seen, a positive transient does not emerge until approximately 200 fs after the first pump pulse, and the magnitude of the change continues to increase as more of the material is transformed into the metallic state. This suggests that the establishment of a quasiequilibrated metallic state is a significantly slower process than the loss of the M_1-phase restoring forces. The loss of M_1-phase modes occurs during the excitation process, which is significantly quicker than the 200 fs observed for the formation of the metallic state properties. We have also measured the temperature dependence of the pump probe signal in the metallic phase at a probe wavelength of 800 nm (data not shown) and found that the magnitude of the signal did not vary significantly with base temperature. This demonstrates that the early dynamics of VO_2, when excited above threshold, cannot be considered simply as arising from a hot metallic phase, but from a distinct nonthermal state far from equilibrium.

V. DISCUSSION

These results show that the photoinduced IM transition is a complex process that occurs over multiple time scales, the measured dynamics of which is significantly dependent on the excitation fluence used and wavelength at which they are probed. By probing the broadband dynamics in this system and performing pump-probe measurements on the transient state of VO_2 during the IM transition, we have clarified the nature of some of these dynamical processes.

By analyzing the response of the lattice, we have shown that the phonon modes that define the M_1 phase are lost on the time scale of the exciting laser pulse. However, the establishment of the equilibrium metallic R phase properties does not occur on the same time scale as the observed change in the lattice potential. By performing pump-probe measurements on the transient state of the system, we observe that a metallic-like response does not emerge until a few-hundred-femtosecond to picosecond have elapsed, suggesting that the properties of the system are in a strong state of flux, with different subsystems evolving on different time scales. Similarly, electron diffraction measurements also show different time scales and that the long-range crystallographic order of the R phase is established on a time scale of several 10–100 picoseconds due to the slow shear motion of the V ions.[13]

This suggests that the nonequilibrium state of VO_2, shortly after photoexcitation, should not be thought of as either the M_1-insulating or R-metallic phase, as the properties that define these phases are not fully established on these time scales. In the saturation regime, the large photoexcitation of charges triggered by the pump pulse is sufficient to modify the symmetry of the lattice potential so that the phonon modes of the M_1 phase are no longer defined. This then acts as the force that drives the system to the metallic R state, however, the evolution of the electronic and lattice system does not appear to be concomitant. The time evolution of the pump-probe signal of the transient state suggests that the R-phase electronic response is established within a few picoseconds, whereas the complete R-phase structure continues to evolve on even longer time scales as measured by electron diffraction.[13] Yet, once established, the R phase remains stable as the deposited energy is more than enough to locally heat the system above the transition temperature, and thus only returns to the M_1 phase after sufficient time for thermal diffusion and cooling. Further pump probe measurements of this cooling process may also provide interesting insights into the nature of the reverse of this transition, in particular, dynamics arising from spontaneous symmetry breaking associated with the reduction of symmetry from the R phase back to the M_1 phase.[38]

Unlike previous experiments in VO_2 that measured coherent oscillations in the low-frequency conductivity, we do not observe a single mode at 6 THz as reported in Refs. 7 and 9. The observation of only a single frequency was interpreted as resulting from a transition to a broken-dimer state, where photoexcitation changes the potential energy surface of local vanadium dimers. This ground state of the new potential energy was believed to have the undistorted structure, and thus the oscillations represented a new mode as the system oscillated around the new equilibrium position. However, we clearly observe the two modes that define the monoclinic phase, when exciting below the transition threshold, demonstrating that the phonon modes that define the M_1 phase can be observed in an excited state. In addition, we do *not* observe any coherent oscillations when exciting above threshold and find no evidence for coherent oscillations in a broken dimer state. We believe that these differences can be reconciled by noting that static Raman scattering measurements on samples of VO_2 that have an oxygen rich concentration, which can arise due to exposure to air, show a shift from the double peak spectra we observe at 5.7 and 6.7 THz, to a single 6-THz peak. Thus we believe that the oscillations reported in Refs. 7 and 9 still arise from VO_2 with M_1 crystal symmetry, albeit with a richer oxygen concentration, and cannot be ascribed simply to photoinduced broken dimers.

This view is also supported by recent static experiments. Total x-ray scattering measurements on bulk samples have excluded the local dimer description of the equilibrium phase transition[39] and the temperature and pressure phase diagram of VO_2 show that the equilibrium transition pathway is strongly influenced by the strain in the material and can generate additional monoclinic M_2 and triclinic T intermediate phases.[33] These additional phases may be particularly important for thinner films, in which the strain from substrate mismatch plays a stronger role in determining the material properties. The thick films used in our experiments (200 nm) should minimize

these effects, providing a more bulklike response. Still, these additional phases may also play a significant role in the dynamics of the phase transition even in our samples as, if only a small region of the film is transformed, the volume mismatch between the M_1 and R phases could result in a significant stress/strain profile, which may also drive transitions to the other phases found in VO_2.[20] If such local phase separation occurs in the time domain, it may be accessible by spatially resolving the pump-probe signal as the phonon spectra are different in the different phases.

Our results extend the previously suggested picture of the structural bottleneck reported in Ref. 17 for the ultrafast transition in VO_2. We do not observe a single time scale that can be said to limit the transition as all time scales observed are strongly dependent on the pump fluence and the wavelength region probed, nor can the observed time scales be assigned to a particular mode of the M_1 phase. Instead, we show that the phonon modes of the monoclinic phase are no longer defined within the time scale of the pump pulse. However, we believe that these results are still consistent with a modified Peierls description as the electronic excitation directly changes the lattice potential, which can also rapidly drive a phase transition on an ultrafast time scale that is not set by the equilibrium response of the lattice. We measure a range of time scales that correspond to the different processes occurring during the transition which show that there is a separation of the structural and electronic dynamics. As the time scales measured depend on the probed wavelength, we believe that our experiments show that care needs to be applied when trying to determine the nature of the phase transition based purely on the time scale of a single process, as different facets may evolve on different time scales and affect different spectral properties at different rates.

Finally, the structural response of VO_2 when driven into the saturation regime, i.e., where a complete structural phase transition results, is fundamentally different to those found in highly excited materials where no phase transition results, such as charge transfer compounds,[40] organic solids,[41,42] or bismuth. In these cases, photoexcitation increases the dephasing rate and softens the phonon modes, but does not result in an underlying change in the symmetry of the lattice potential on an ultrafast time scale.[43–45] VO_2, on the other hand, shows a distinct change in the number of phonon modes when excited above threshold, demonstrating that the laser pulse has changed the lattice potential symmetry. The technique to measure the structure through the coherent phonon spectrum can be applied to any material with Raman active phonons and will be particularly useful for studying the structural dynamics of manganites, which also exhibit a rich variety of solid-solid phase transitions.[46–48]

ACKNOWLEDGMENTS

S.W. acknowledges support from the Alexander von Humboldt Foundation. Research at Vanderbilt was supported by the National Science Foundation (ECCS-0801985).

*Corresponding author: simon.wall@icfo.es

[1] F. J. Morin, Phys. Rev. Lett. **3**, 34 (1959).
[2] J. B. Goodenough, J. Solid State Chem. **3**, 490 (1971).
[3] A. Zylbersztejn and N. F. Mott, Phys. Rev. B **11**, 4383 (1975).
[4] V. Eyert, Phys. Rev. Lett. **107**, 016401 (2011).
[5] F. Iori, M. Gatti, and A. Rubio, Phys. Rev. B **85**, 115129 (2012).
[6] W. R. Roach and I. Balberg, Solid State Commun. **9**, 551 (1971).
[7] C. Kübler, H. Ehrke, R. Huber, R. Lopez, A. Halabica, R. F. Haglund, and A. Leitenstorfer, Phys. Rev. Lett. **99**, 116401 (2007).
[8] D. J. Hilton, R. P. Prasankumar, S. Fourmaux, A. Cavalleri, D. Brassard, M. A. El Khakani, J. C. Kieffer, A. J. Taylor, and R. D. Averitt, Phys. Rev. Lett. **99**, 226401 (2007).
[9] A. Pashkin, C. Kübler, H. Ehrke, R. Lopez, A. Halabica, R. F. Haglund, R. Huber, and A. Leitenstorfer, Phys. Rev. B **83**, 195120 (2011).
[10] A. Cavalleri, H. H. W. Chong, S. Fourmaux, T. E. Glover, P. A. Heimann, J. C. Kieffer, B. S. Mun, H. A. Padmore, and R. W. Schoenlein, Phys. Rev. B **69**, 153106 (2004).
[11] A. Cavalleri, M. Rini, H. H. W. Chong, S. Fourmaux, T. E. Glover, P. A. Heimann, J. C. Kieffer, and R. W. Schoenlein, Phys. Rev. Lett. **95**, 067405 (2005).
[12] A. Cavalleri, C. Tóth, C. W. Siders, J. A. Squier, F. Ráksi, P. Forget, and J. C. Kieffer, Phys. Rev. Lett. **87**, 237401 (2001).
[13] P. Baum, D.-S. Yang, and A. H. Zewail, Science **318**, 788 (2007).
[14] M. Hada, K. Okimura, and J. Matsuo, Phys. Rev. B **82**, 153401 (2010).
[15] M. Hada, K. Okimura, and J. Matsuo, Appl. Phys. Lett. **99**, 051903 (2011).
[16] M. Rini, Z. Hao, R. W. Schoenlein, C. Giannetti, F. Parmigiani, S. Fourmaux, J. C. Kieffer, A. Fujimori, M. Onoda, S. Wall, and A. Cavalleri, Appl. Phys. Lett. **92**, 181904 (2008).
[17] A. Cavalleri, T. Dekorsy, H. H. W. Chong, J. C. Kieffer, and R. W. Schoenlein, Phys. Rev. B **70**, 161102 (2004).
[18] G. Sciaini, M. Harb, S. G. Kruglik, T. Payer, C. T. Hebeisen, F.-J. Meyer zu Heringdorf, M. Yamaguchi, M. Horn-von Hoegen, R. Ernstorfer, and R. J. D. Miller, Nature (London) **458**, 56 (2009).
[19] S. Wall, D. Wegkamp, L. Foglia, K. Appavoo, J. Nag, R. F. Haglund, Jr, J. Stähler, and M. Wolf, Nat. Commun. **3**, 721 (2012).
[20] A. C. Jones, S. Berweger, J. Wei, D. Cobden, and M. B. Raschke, Nano Lett. **10**, 1574 (2010).
[21] H. W. Verleur, A. S. Barker, and C. N. Berglund, Phys. Rev. **172**, 788 (1968).
[22] J. Nag and R. F. Haglund, J. Phys.: Condens. Matter **20**, 264016 (2008).
[23] D. Wegkamp, D. Brida, S. Bonora, G. Cerullo, J. Stähler, M. Wolf, and S. Wall, Appl. Phys. Lett. **99**, 101101 (2011).
[24] S. Wall, D. Brida, S. R. Clark, H. Ehrke, D. Jaksch, A. Ardavan, S. Bonora, H. Uemura, Y. Takahashi, T. Hasegawa, H. Okamoto, G. Cerullo, and A. Cavalleri, Nat. Phys. **7**, 114 (2011).
[25] C. Giannetti, F. Cilento, S.-D. Conte, G. Coslovich, G. Ferrini, M. Molegraaf, H. Raichle, R. Liang, H. Eisaki, M. Greven, A. Damascelli, D. van der Marel, and F. Parmigiani, Nat. Commun. **2**, 353 (2011).

[26]S. Dal Conte, C. Giannetti, G. Coslovich, F. Cilento, D. Bossini, T. Abebaw, F. Banfi, G. Ferrini, H. Eisaki, M. Greven, A. Damascelli, D. van der Marel, and F. Parmigiani, Science **335**, 1600 (2012).

[27]S. K. Sundaram and E. Mazur, Nat. Mater. **1**, 217 (2002).

[28]Using the bulk values reported in Ref. 21, the penetration depth at 800 nm is 180 nm and the penetration depth at 525 nm is 179 nm. However, these values may strongly depend on film quality.

[29]The threshold values at 525 and 800 nm were measured to be 4.9 and 6.1 mJ cm^{-2}, respectively.

[30]H. J. Zeiger, J. Vidal, T. K. Cheng, E. P. Ippen, G. Dresselhaus, and M. S. Dresselhaus, Phys. Rev. B **45**, 768 (1992).

[31]It should be noted that the force may not necessarily result from excited electrons and other descriptions can lead to the same effect. See Ref. 30 for details.

[32]P. Schilbe, Physica B: Condensed Matter **316-317**, 600 (2002).

[33]J. M. Atkin, S. Berweger, E. K. Chavez, M. B. Raschke, J. Cao, W. Fan, and J. Wu, Phys. Rev. B **85**, 020101 (2012).

[34]H.-T. Kim, Y. W. Lee, B.-J. Kim, B.-G. Chae, S. J. Yun, K.-Y. Kang, K.-J. Han, K.-J. Yee, and Y.-S. Lim, Phys. Rev. Lett. **97**, 266401 (2006).

[35]In the low-fluence data, $\tau_{1/2}$ is equal to zero and w is related to the pulse duration.

[36]S. A. Kovalenko, A. L. Dobryakov, J. Ruthmann, and N. P. Ernsting, Phys. Rev. A **59**, 2369 (1999).

[37]In Ref. 19, we also ruled out phonon oscillations as the origin of the spike, however, other explanations, such as a prepulse cannot be completely excluded.

[38]R. Yusupov, T. Mertelj, V. V. Kabanov, S. Brazovskii, P. Kusar, J. Chu, I. R. Fisher, and D. Mihailovic, Nat. Phys. **6**, 681 (2010).

[39]S. A. Corr, D. P. Shoemaker, B. C. Melot, and R. Seshadri, Phys. Rev. Lett. **105**, 056404 (2010).

[40]M. Trigo, J. Chen, M. P. Jiang, W. L. Mao, S. C. Riggs, M. C. Shapiro, I. R. Fisher, and D. A. Reis, Phys. Rev. B **85**, 081102 (2012).

[41]S. Iwai, Y. Ishige, S. Tanaka, Y. Okimoto, Y. Tokura, and H. Okamoto, Phys. Rev. Lett. **96**, 057403 (2006).

[42]H. Uemura and H. Okamoto, Phys. Rev. Lett. **105**, 258302 (2010).

[43]D. M. Fritz *et al.*, Science **315**, 633 (2007).

[44]M. Hase, K. Mizoguchi, H. Harima, S. Nakashima, M. Tani, K. Sakai, and M. Hangyo, Appl. Phys. Lett. **69**, 2474 (1996).

[45]M. Hase, M. Kitajima, S.-i. Nakashima, and K. Mizoguchi, Phys. Rev. Lett. **88**, 067401 (2002).

[46]S. Wall, M. Rini, S. Dhesi, R. Schoenlein, and A. Cavalleri, IEEE J. Sel. Top. Quantum Electron. **18**, 81 (2012).

[47]P. Beaud, S. L. Johnson, E. Vorobeva, U. Staub, R. A. D. Souza, C. J. Milne, Q. X. Jia, and G. Ingold, Phys. Rev. Lett. **103**, 155702 (2009).

[48]H. Ichikawa, S. Nozawa, T. Sato, A. Tomita, K. Ichiyanagi, M. Chollet, L. Guerin, N. Dean, A. Cavalleri, S. Adachi, T. Arima, H. Sawa, Y. Ogimoto, M. Nakamura, R. Tamaki, K. Miyano, and S. Koshihara, Nat. Mater. **10**, 101 (2011).